Exploration and Sizing of a Large Passenger Aircraft with Distributed Ducted Electric Fans

Alessandro Sgueglia, Peter Schmollgruber, Nathalie Bartoli, Olivier Atinault, Emmanuel Bénard, Joseph Morlier

Exploration and Sizing of a Large Passenger Aircraft with Distributed Ducted Electric Fans

Alessandro Sgueglia*, Peter Schmollgruber†, Nathalie Bartoli†
ONERA - The French Aerospace Lab
2 avenue Edouard Belin, 31055 Toulouse, France

Olivier Atinault‡
ONERA - The French Aerospace Lab
8 rue des Vertugadins, 92190 Meudon, France

Emmanuel Benard§
ISAE - Institut Supérieur de l'Aéronautique et de l'Espace
10 avenue Edouard Belin, 31055 Toulouse, France

Joseph Morlier¶
Institut Clément Ader (ICA), CNRS, ISAE-Supaero, UPS, INSA, Mines-Albi
3 rue Caroline Aigle, 31400 Toulouse, France

In order to reduce the CO_2 emissions, a disruptive concept in aircraft propulsion has to be considered. As studied in the past years hybrid distributed electric propulsion is a promising option. In this work the feasibility of a new concept aircraft, using this technology, has been studied. Two different energy sources have been used: fuel based engines and batteries. The latters have been chosen because of their flexibility during operations and their promising improvements over next years. The technological horizon considered in this study is the 2035: thus some critical hypotheses have been made for electrical components, airframe and propulsion. Due to the uncertainty associated to these data, sensivity analyses have been performed in order to assess the impact of technologies variations. To evaluate the advantages of the proposed concept, a comparison with a conventional aircraft (EIS 2035), based on evolutions of today's technology (airframe, propulsion, aerodynamics) has been made.

Nomenclature

AC	Alternate Current
A/C	Aircraft
ANOVA	Analysis of Variance
C	Torque
C_T	Thrust coefficient
CE	Conventional Engine
CoG	Center of Gravity
C_D	Drag coefficient
C_l	2D lift coefficient

*Ph.D. candidate, ISAE Supaero & ONERA, Information Processing and Systems Department, AIAA Student Member
†Research Engineer, Information Processing and Systems Department, AIAA Member.
‡Research Engineer, Aerodynamic, Aeroelasticity and Acoustic Department.
§Professor, Aircraft Design, AIAA Member.
¶Professor, Structural Mechanics, AIAA Member.

C_L	3D lift coefficient
DC	Direct current
DEP	Distributed Electric Propulsion
DoD	Depth of Discharge
EIS	Entry Into Service
EM	Electric Motors
E/m	Specific energy density
E/V	Energy density
FC	Fuel Consumption
ΔH	Variation of total enthalpy
$\dot{m}$	Mass flow
MDA	Multidisciplinary Design Analysis
MDO	Multidisciplinary Design Optimization
MFW	Maximum Fuel Weight
MLG	Main Landing Gear
MLW	Maximum Landing Weight
MTOW	Maximum Takeoff Weight
N	Number of engines
OEI	One Engine Inoperative
OWE	Operational Weight Empty
p	Pressure
P	Power
PL	Payload
P/m	Specific power density
P/V	Power density
r	Radius
R	Gas constant for air
S	Surface
SM	Static Margin
SoC	State of Charge
T	Thrust
TLAR	Top Level Aircraft Requirements
xDSM	eXtended Design Structure Matrix
$\underline{x}$	Coordinate of a generic component
$\underline{y}$	Vector containing the parameters of a generic component
V	Volume
V_∞	Freestream velocity

Subscript

$batt$	Battery
$blow$	Blowing
$diss$	Dissipated
EM	Electric Motor
fan	Fan
gen	Generator
IC	Inverter/Converter
ref	Reference parameter
s	Static parameter
t	Total parameter
w	Wing

Greek letters

α	Angle of attack
γ	Gas heat capacity ratio
δ	Power rate
θ	Temperature

η	Efficiency
ρ	Density
Ω	Rotational speed, in rpm

I. Introduction

In the next decades, due to the cost of fuel and the increasing number of aircraft flying everyday, the world of aviation will cope with more stringent environmental constraints and traffic density increase. Both ACARE (Advisory Council or Aviation Research and Innovation in Europe)[1] and NASA[2] published their targets in terms of environmental impact within the next years. In Table 1 the noise, emissions and energy consumption reduction according to ACARE for the next years are reported: the fuel and energy consumption have to be drastically reduced to meet the 2050 goals.

Table 1. ACARE targets for the next years[1]

Target parameter [%]	**2025**	**2035**	**2050**
Noise	-10.0	-11.0	-15.0
Emissions	-81.0	-84.0	-90.0
Fuel\Energy consumption	-49.0	-60.0	-75.0

To achieve these objectives, disruptive changes at the aircraft level have to be made. Fostered by the progress made in the automotive industry, aeronautics found an interest in hybrid propulsion. An idea is to merge this concept and distributed propulsion, where the engines are distributed along the wing. As shown by Kirner[3] and Ko et al.,[4] distributed propulsion increases performance in fuel consumption, noise, emission and handling qualities. The resulting Distributed Electric Propulsion (DEP) technology has been applied for different aircraft configuration (such as the N+3 Aircraft generation from NASA[5]): results show a drag reduction (which leads to a minor fuel consumption) and also a better efficiency due to the aero propulsive effects.

This work presents the exploration and the sizing of a large passenger aircraft with distributed electric ducted fans, EIS 2035. The objective is to carry out a Multidisciplinary Design Analysis (MDA) in order to consider all the coupling between the disciplines: airframe, hybrid electric propulsion and aerodynamics. The aero propulsive effects are also considered, in order to converge towards a disruptive concept.

In the first part of the paper the proposed concept is described, then the propulsive chain architecture is presented, including a review of the key components and their models. The second part is dedicated to their integration in the in-house aircraft sizing code developed by ONERA and ISAE-Supaero, identified as FAST.[6] Then the design mission is presented, and the hypothesis for the 2035 technology horizon are discussed. Finally, the performance of the integrated design are presented, and the conclusions regarding the feasibility of such vehicle are reported.

II. Electric hybrid aircraft concept

The aircraft definitive concept is shown in Fig. 1: for the modelisation it has been used OpenVSP,[7] a free tool for visualization and VLM computation. New components are added to the aircraft architectures:

- Turbogenerators, which are the ensemble of a fuel burning engine and a converter device;
- Batteries (not shown in figure) which provide electric power and are located in the cargo;
- Electric motor and ducted fan, in the nacelle on the wing upper surface;
- DC/DC and DC/AC converter (called respectively converter and inverter[8]) in order to provide the current in the right mode and at the same voltage;

- Cables for the current transport, including a cooling system and protections.

Detailed models of each component are described in the next section. The wing-body airframe is the usual "tube and wing" configuration, and no changes on that part have been done. For the engine positions, different choices are possible:[9] upper-wing trailing edge engines, lower-wing leading edge engines and imbedded engines. In this work they are located in the upper part of the wing, at the trailing edge. This allows some advantages in terms of blowing: from an internal project in the frame of the EU program CleanSky 2,[10] it has been estimated the 2D maximum lift coefficient in the zone affected by the engines varies from 4 to 5. For the results presented later it has been used the mean value of 4.5. This effect has three main advantages:

- If the approach speed constraint is used for the wing sizing, the wing surface is reduced.
- High-lift devices are no more needed for takeoff and landing, leading to a minor wing weight.
- It is possible to have a shorter takeoff length.

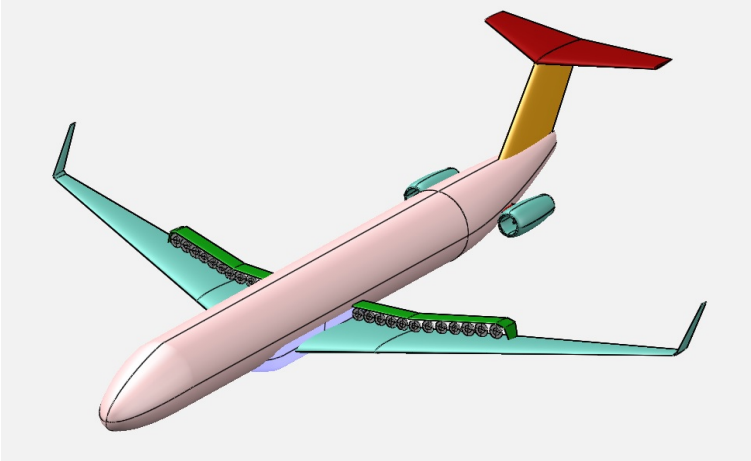

Figure 1. Hybrid aircraft concept proposed with distributed electric ducted fan - modelisation in OpenVSP[7]

Also, in previous works[9] the engines are mounted near the tip, since it is on that zone the stall begins and a higher C_L is needed. In this concept they are located on the inner part in order to not increase the structure at the tip: a twist has to be added in order to make the stall begin in the center part. The motors also provide some moment which partially balance the bending at the wing root: from an internal work at ONERA, it has been estimated that the impact of the engine position on the wing weight is of 5%.

Another advantage of the DEP architecture is that the EM weight is reduced. In fact, the One Engine Inoperative (OEI) condition (which is assumed as critical case for the design) is less stringent, as shown by Steiner et al.:[11] in case of OEI condition, the supplementary power (and thus also thrust) required by the other engines is smaller; in particular the total power of a single motor increases with the ratio of $\frac{N}{N-1}$, being N the number of engines. It is clear that, when the number of engines increases, the effect of the OEI condition becomes negligable, and the weight of each motor decreases. Aircraft is also sized in order to have all the EM working, even if one of the energy source is inoperative.

Regarding the energy sources, the generators are located at the rear, on the fuselage, in order to reduce the pylons wetted area and the interferences with the wing. The batteries are instead located in the cargo zone, half of them ahead the wing and the other half back the wing. This choice has been made because it is expected to find the center of gravity in proximity of the wing, and with this disposition the batteries do not drastically affect its position. Also, due to batteries location (in the cargo), the maximum payload is reduced since only part of the freight is available for luggages. A T-tail configuration has been used for the empennage.

In this work it has been decided to size the aircraft in order to fly fully electric at least to 3000ft. The reason for this choice is that the mean atmospheric boundary layer height is of about 1km (it changes according to the atmospheric condition), and in that region the convective effects create turbulences which mix the air[12] (Fig. 2): when the emissions are in this region, the quality of the air is decreased, meanwhile for greater altitude this effect is no more as relevant as it is in the boundary layer region.

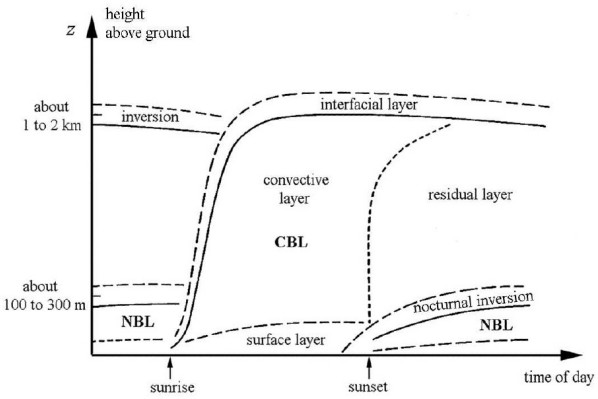

Figure 2. Typical evolution of atmospheric boundary layer during the day. The convective boundary layer extension is shown[12]

III. Propulsive chain architecture

The generic scheme of the propulsive chain is shown in Fig. 3: it is referred to only one half wing, and the number of batteries, generators, EM and fans are not specified since they are variables to be optimized.

In this kind of architecture batteries are coupled with a turbogenerator in order to supply power: they are connected through an electrical node (called bus in this work), thus they can be defined as a serial architecture. Converters are placed after these components in order to bring the current at the right transport voltage. The total power is then transferred to the inverters, which convert DC to AC current, required by electric motors. EM work in parallel; each of them is connected to a ducted fan, which generates thrust. Since all the cables from batteries and generators are connected to the bus, from which the current is then trasported to the EM, they are always operative, even if one energy source being inoperative.

The power available at each step of the chain is also specified in Fig. 3: η is the efficiency of a generic component, $\frac{P}{V}$ the power density, M the Mach number, z the altitude, N the number of electric motors, T the thrust and V_∞ the velocity. In the following sections, each component is detailed.

Power is controlled using two different power rates, one for the batteries and another one for the generators. It is then possible to write:

$$P_{tot} = \delta_{batt} P_{batt2} + \delta_{gen} P_{gen2} \tag{1}$$

having defined the battery and generator power rate as below:

$$\delta_{batt} = \frac{P_{batt}}{P_{batt,max}} \tag{2}$$

$$\delta_{gen} = \frac{P_{gen}}{P_{gen,max}} \tag{3}$$

where $P_{batt,2}$ and $P_{gen,2}$ are defined from Fig. 3. In previous works on hybrid architectures[13,14], an hybrid factor has been defined in order to control how much of the total power had to be supplied by each source. In this work, there is no factor splitting the power required from the two sources: with the law presented in Eq. (1) it is possible to have batteries and generators supply the maximum of their available power at the same time. The advantage offered by this approach is that at takeoff or climb (critical conditions in terms of power required), a failure of one energy source can be easily sustained: in case one of them being inoperative, it is possible to ask more power from the second source.

Finally, the power required by secondary systems (such as the environmental control system, the ice protection system, lighting and so on) have to be considered too: in this work it has been decided to use the estimation done by Seresinhe and Lawson[15] for a More Electric Aircraft concept, similar to A320.

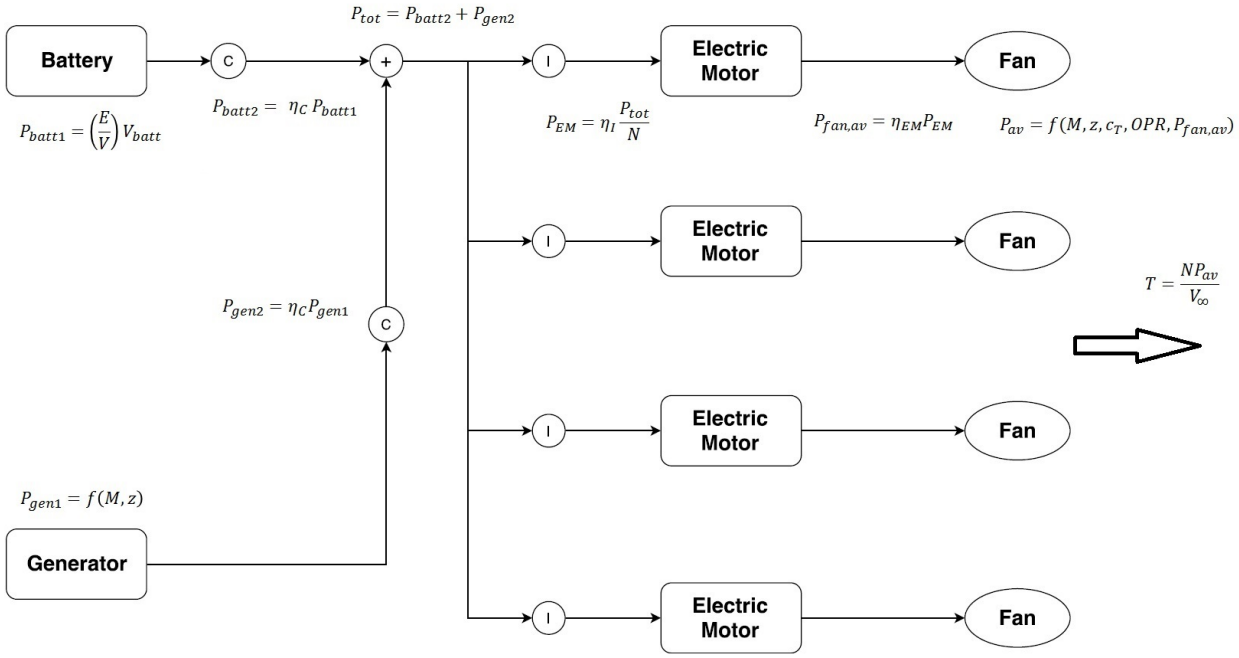

Figure 3. Distributed electric propulsion architecture

A. Gas turbine generator

One of the two power sources is the gas turbine generator: it is composed of a turboshaft engine connected to a generator which converts shaft power to electrical power. The turboshaft has been modeled using GSP (Gasturbine Simulation Program), a software developed at NLR.[16] The scheme is shown in Fig. 4. A single compressor has been used, meanwhile there are two turbines after the combustion chamber: the first is the high speed turbine, directly linked to the compressor, while the second is the low speed turbine. Since it has to produce power, the main outputs are the power and the Power Specific Fuel Consumption (PSFC), which depend on the altitude and the Mach number. The design conditions are reported in Table 2. The turboshaft engine has also been sized in order to supply enough power in case of failure of one energy source in cruise.

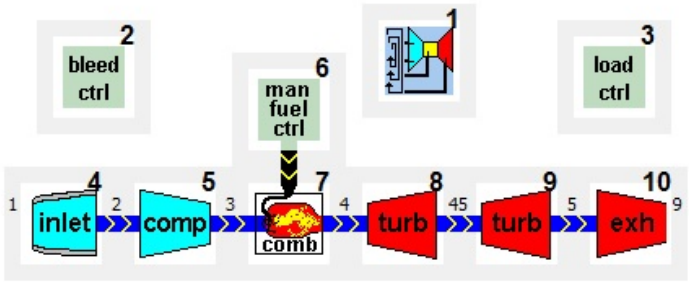

Figure 4. Turboshaft scheme, as modeled in GSP (software developed at NLR)[16]

The gas turbine is not included into the sizing process: once having obtained the curves of power and PSFC from GSP, they are provided to the software FAST and interpolated to get the value of interest. An estimation of the weight is given in the work of Burguburu et al.:[17] it is based on empirical data from a

Table 2. Turboshaft design parameters

Design Mach number	0.70	
Design operating altitude	11000	m
Power at design point	13293	kW
PSFC at design point	0.22	$\mathrm{kg\,kW^{-1}\,h^{-1}}$

large number of existing turboshaft engines.

As previously said, the converter device is mounted on the low speed turbine shaft. The only parameter used for sizing is the power to mass ratio $\left(\frac{P}{m}\right)$, defined as the power converted per unit mass. Starting from this parameter it is possible to estimate the weight:

$$m_{gen} = \frac{P_{gen}}{\left(\frac{P}{m}\right)} \tag{4}$$

where P_{gen} is the power delivered to the device at the design point.

B. Battery

In the proposed architecture, battery is a vital component as it is a main source of power as it introduces significant weight to the entire system. There are different types of battery available (such, for example, Li-Ion or Li-S[18]): in this work it has been decided to use a Li-Ion battery type. A battery is fully defined by a set of five parameters:[13,19,20]

- Specific energy density $\left(\frac{E}{m}\right)$, which represents how much energy can be stored in a battery per unit mass (in $\mathrm{W\,h\,kg^{-1}}$);
- Energy density $\left(\frac{E}{V}\right)$, which represents how much energy can be stored in a battery per unit volume (in $\mathrm{W\,h\,L^{-1}}$);
- Specific power density $\left(\frac{P}{m}\right)$, which represents how much power can be delivered per unit mass (in $\mathrm{kW\,kg^{-1}}$);
- Power density $\left(\frac{P}{V}\right)$, which represents how much power can be delivered per unit volume (in $\mathrm{kW\,L^{-1}}$);
- Density (ρ), which represents the mass per unit of volume (in $\mathrm{kg\,m^{-3}}$).

These variables are not independent of each others, but only three of them are necessary to compute the others ones. In this work, a battery is defined by its specific energy density, specific power density and density. Missing values are calculated as follows:

$$\left(\frac{E}{V}\right) = \rho\left(\frac{E}{m}\right) \tag{5}$$

$$\left(\frac{P}{V}\right) = \rho\left(\frac{P}{m}\right) \tag{6}$$

The energy stored and the maximum power which can be delivered by the battery are then computed:

$$E_{batt} = \left(\frac{E}{m}\right) m_{batt} = \left(\frac{E}{V}\right) V_{batt} \tag{7}$$

$$P_{max,batt} = \left(\frac{P}{m}\right) m_{batt} = \left(\frac{P}{V}\right) V_{batt} \tag{8}$$

where m_{batt} is the battery mass and V_{batt} the battery volume. For monitoring the state of the battery, the state of charge (SoC) has to be defined: it is the ratio between the remaining energy E at a certain time (t) and the total stored energy E_{batt}. The complement of SoC is defined as the Depth of Discharge (DoD).

$$SoC = \frac{E(t)}{E_{batt}} = 1 - \frac{E_{cons}(t)}{E_{batt}} \tag{9}$$

$$DoD = \frac{E_{cons}(t)}{E_{batt}} = 1 - SoC \tag{10}$$

Due to safety reasons, the SoC can not be under a certain limit, which in general depends on the battery type. For a Li-Ion battery the minimum limit for the SoC is 20%; therefore the following constraint will be used in the sizing process:

$$SoC_{final} = 1 - DoD_{final} \geq 0.2 \tag{11}$$

C. Electric motor

Electric motors are the other main components of the hybrid propulsion: they convert electrical power to mechanical power. The high reliability allows to work at very high efficiency; furthermore, as opposed to traditional combustion engine, their efficiency is independent from the altitude, which represents the main advantage.[19] Performance of these electric motors is determined by their torque and rotational speed charateristics. In this work it has been decided to use AC current based motors, since they are lighter than DC current based. Electric motors have also a very high efficiency (about 0.95); inefficiencies can be caused by various factors and are of different types[19] (but a complete analysis of them is beyond the scope of this work, in which only the total efficiency is defined).
The major requirement for electric motors is the power to mass ratio, defined as the power that delivered per mass unit. Once the maximum power required by the electric motor is known, it is possible to estimate its weight:

$$m_{EM} = \frac{P_{max,EM}}{\left(\frac{P}{m}\right)} \tag{12}$$

In subsequent steps the rotational speed and the torque are computed according to the fan requirement, and the motor is then fully defined.

D. DC/DC and DC/AC transformers

In order to convert current within the energy chain, converters and inverters are used. Performance of these devices depends on their efficiency, which is around 0.9. Since the architectures of inverter and converter are similar, it is possible to compute directly their total weight with the equation

$$m_{IC} = \frac{P_{inverter}N_{EM} + P_{converter}N_{gen} + P_{converter}N_{batt}}{\left(\frac{P}{m}\right)} \tag{13}$$

where $\left(\frac{P}{m}\right)$ is the power to mass ratio, N_{EM} the number of electric motors, N_{gen} the number of generators and N_{batt} the number of batteries.

E. Cables

The cables have to transport current from one device to another within the hybrid architecture. They are sized in order to carry a certain current, which must be below the maximum allowed threshold. The current, and so the sizing, depends on the voltage used for the transport. First the current which flows through a cable is computed as

$$i = \frac{P}{\Delta V} \tag{14}$$

Then a check has to be done in order to be sure that value is lower than the maximum current. If it is not, more cables have to be installed; the number is computed dividing the value of current with the maximum one:

$$N_{cable} = \left[\frac{i}{i_{max}}\right] \tag{15}$$

where the square brackets represents the integer part of $\frac{i}{i_{max}}$. Finally, according to EM, generators and batteries positions, it is possible to estimate the cable length and so the weight:

$$m_{cable} = N_{cable} \left(\frac{m}{L}\right) L_{cable} \tag{16}$$

where $\frac{m}{L}$ is the cable linear density. Installation and Healt Monitoring System have to be included in the weight calculation: preliminary works at ONERA[10] show an increasing in weight of 30% for the installation and of 5% for the HMS. Typical values for the cables' parameters are reported in Table 3.[21]

Table 3. Values used for the cables sizing

i_{max}	360	A
ΔV	2160	V
m/L	1.0	$\mathrm{kg\,m^{-1}}$

F. Cooling system

All the components have their efficiency: this means that not all the power generated by batteries or generators is converted into electrical power, but part of them is converted into heat. It consists of two different devices: heat exchanger and air cooling systems. The first are devices which surrounds the cables and artificially dissipate the power. The amount of power to dissipate is:

$$P_{diss} = (1 - \eta_{batt})\, P_{batt,max} N_{batt} + (1 - \eta_{gen})\, P_{gen,max} N_{gen} + (1 - \eta_{EM})\, P_{EM,max} N_{EM} \tag{17}$$

The heat exchangers introduce a penalty in mass: in the framework of an internal project at ONERA, the penalty has been estimated to be 1t.[10] This value is based also on the work of Anton.[22]

The air cooling system is used instead to have cold air that circulates into the system: it consists of some air inlet placed on the fuselage. It does not introduce weight but a penalty on the drag coefficient:[23] in the same internal project mentioned, the impact has been estimated to be of 5% on the C_D. Penalties due to the cooling system are summed up in Table 4.

Table 4. Penalties due to the cooling system considered in this work (estimation from an internal work at ONERA)

Mass	+1	t
$\mathbf{C_D}$	+5	%

G. Fan

The ducted fans are the last devices in the energy chain: they are directly connected to the electric motor. The design point for the preliminary sizing has been chosen as the beginning of the cruise.

As the fans are directly connected to electric motors, the torque and rotational speeds have to be the same for both: if the motor torque is too small, a resize of the fan has to be carried out, or a gearbox must be added. In Fig. 5 the scheme of a ducted electric fan is shown, meanwhile in Fig. 6 a 3D rendering is given, where the elements are drawn separately in order to understand the architecture. Due to technological limits, there is a minimum for the fan diameter: if it is too small, it is not possible to design the fan. In order to avoid this situation, the operating Mach number should not exceed the value of 0.7. In Appendix B the fan sizing, based on isoentropic equations, is fully described.

Since the air passes through the fan, the wetted area of the duct is relevant for aerodynamic calculations. It is computed considering the total area of the external duct, the disk created by the actuator, the central duct and the total area of the electric motor.

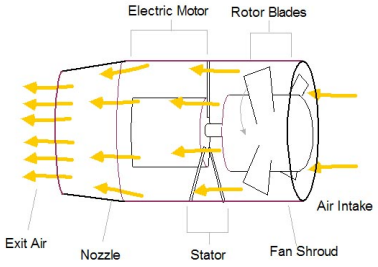

Figure 5. General scheme of a ducted electric fan with its different parts

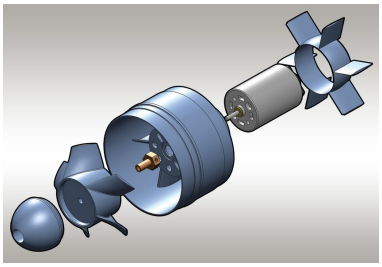

Figure 6. Three-dimensional rendering of a ducted electric fan

IV. Description of the sizing tool FAST

FAST, which stands for Fixed-wing Aircraft Sizing Tool,[6] is an aircraft sizing code, fully developed in Python 2.7, based on the point mass approach to estimate the required fuel consumption for a given set of Top Level Aircraft Requirements (TLAR). It performs a Multidisciplinary Design Analysis (MDA), taking into account different key disciplines: aerodynamics, structure/weight and propulsion. In the traditional version of FAST, there are 19 different modules, divided into three main categories: management, analysis, and wrapper modules. A common .xml file is used both for reading the input and writing the output: it is divided into different sections for geometry, aerodynamics, propulsion and code configuration.

The FAST code has been modified in order to consider also the hybrid architecture sizing. New modules have been added, into the new category "HybridDEP"; here below there is a rapid description:

- **Battery.py**: this module contains the battery model and the functions used for computing the actual SoC, the weight, the volume, the energy and the maximum power available. Battery sizing is also included.
- **Cable.py**: this module contains the definition of the cable function used for computing the maximum current, the diameter and the weight.
- **DuctedFan.py**: this module contains the functions used for sizing the ducted fan and computing the power required for the condition of interest.
- **ElectricMotor.py**: this module contains the definition of the electric motor and the function used for its sizing.
- **HybridEngine.py**: this module is the main module for the propulsion, since it calls the components' modules for computing both the power and the thrust (as in Fig. 3) according to the actual requirement during flight phase and the PSFC to estimate the fuel consumption.

The standard mass breakdown module using the French norm AIR 2001/D[24] has also been modified. Since it considers only a classical "tube and wing" configuration, there are no references on the hybrid architecture, such as batteries or cables. Thus five new elements have been added in the propulsion category.

The detailed structure is presented in appendix A (Table 16). Finally, two new sections in the .xml input file have been added: one contains all the parameters for the hybrid distributed electric propulsion, while the other contains an estimation of the secondary systems power.

The FAST workflow is presented in Fig. 7: since from a method's point of view it can be considered as a MDA, an eXtended Design Strucutre Matrix (xDSM) scheme[25] has been used to describe the main process. Under this format, each rectangular box represents an analysis (e.g. a function or computational code). Input variables related to the analysis are placed vertically while outputs are placed horizontally. Thick gray lines represent data dependencies whereas thin black lines represent process connections. The order of execution is established by the component number. Finally, the superscript notation defined by Lambe et al.[25] has been used.

Algorithm 1 details the different steps based on the input given by the work of Pornet et al.[13] and Cinar et al.,[14] which describe a sizing process for electric aircrafts. Respect to the original version, a new analysis is added at step 2; all the other blocks have been indirectly modified due to the presence of the new propulsive architecture.

Algorithm 1 FAST algorithm

Require: Initial design parameters (TLAR)

Ensure: Sized aircraft, drag polars, masses, design mission trajectory

0: Initialize the values. Estimate weight, wing surfaces initial values, using methods from ISAE & Airbus design manual,[26] as initialization of DEP components.

repeat

1: Initialize the loop.

2:Battery sizing. Batteries are sized respect to two different criteria: the power at the takeoff and the energy consumed; the latter is divided by 0.8 in order to consider the 20% safety margin of SoC. Using Eq. (7) and Eq. (8), battery volume is computed, then the maximum value is taken. Finally, using the same equations, power and energy available are defined. At the first iteration the initial value of volume from step 0 is used, since there is no information about the energy consumption.

3: Wing sizing. Wing area is sized with respect to fuel capacity and approach speed. As for the battery, at the first iteration no wing sizing is performed, as there is no information about the fuel consumption.

4: Compute initial geometry.

5: Resize the geometry in order to match the center of gravity and stability constraints.

6: Aerodynamic calculation.

7: Mass breakdown calculation. For the DEP components, the weight estimation is based according to values from previous loop;

8: Design mission simulation. The mission includes: take off, initial climb (up to 1500ft), climb to cruise altitude, cruise, descent, alternate flight of 200NM, 45 minutes of holding, landing and taxi in. For the cruise two approaches are possible (step and cruise climb); more details will be provided in section V. For the Hybrid-Electric concept, the balance equation is written in terms of power instead of thrust; at each step the code computes the fuel and energy consumption and updates the aircraft weight and battery SoC.

9: Update the MTOW.

10: Check if the convergence criteria is satisfied; if not proceed to next iteration. The convergence is reached when the relative difference between the Operating Weight Empty (OWE) computed at step 7 and step 8 is less than 0.05%. If this condition is satisfied, the code check that the mission fuel is lower than the maximum fuel that can be stored, as that the battery SoC is greater than 20%: if these conditions are fulfilled, the sizing loop is over, otherwise it proceeds to next iteration.

until $10 \rightarrow 1$: MDA has converged

V. Design mission and sizing parameters

A. Design mission definition

In the FAST code, the design mission is made of two blocks: the first one represents the mission, and the second one is used for computing the reserve, according to certification rules.[6] In particular, the reserve fuel

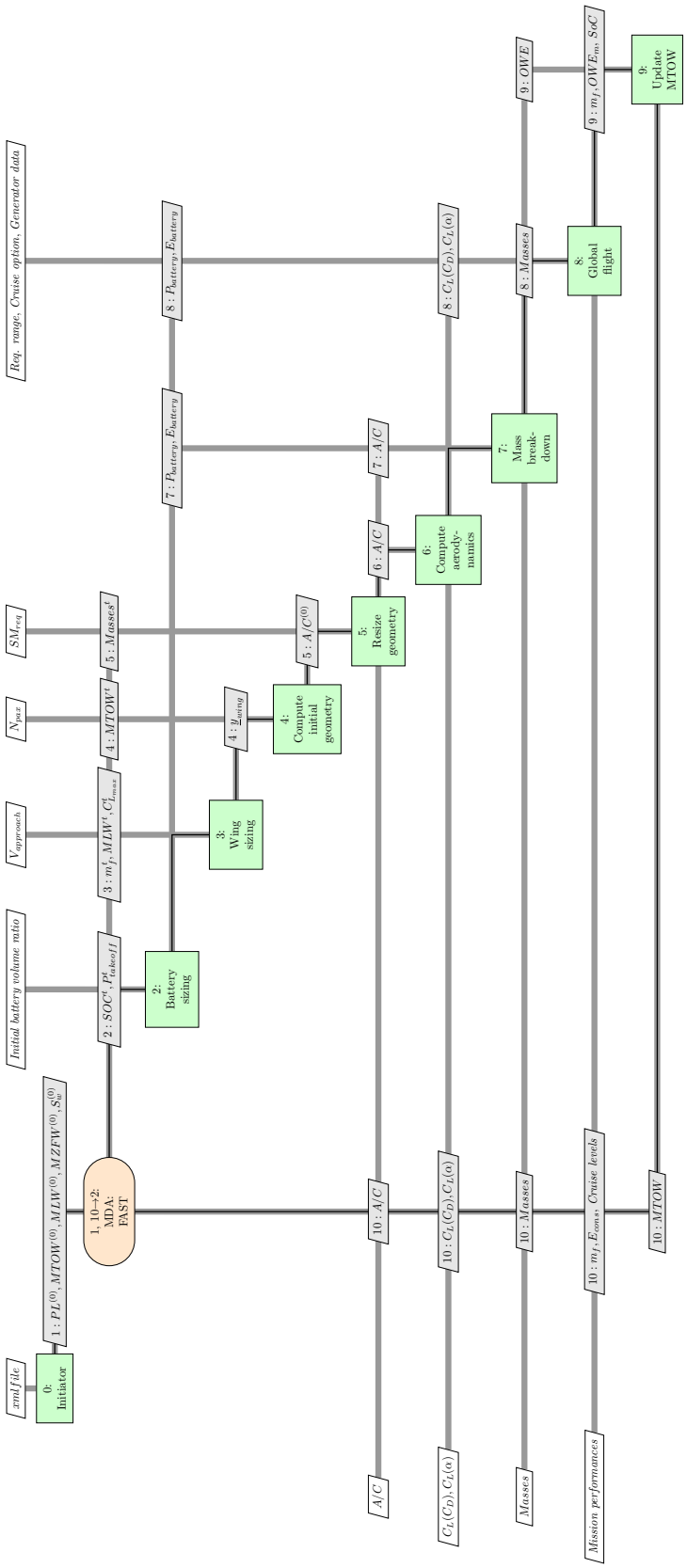

Figure 7. FAST xDSM. Black lines represent the main workflow; thick grey lines represent the data flow, meanwhile green blocks indicate an analysis, grey and white block an input/output data. Algorithm 1 details the MDA.

is computed considering an alternate flight of 200NM and 45 minutes of holding. For the key segment of the mission (cruise), two different approaches can be selected: the step climb mission and the cruise climb mission.[8] In the first case the cruise starts at the optimal altitude (computed by the code), which is kept constant until the code computes is more efficient to climb at a higher level with a step climb of 2000ft. In the second case the aircraft is always at the point of maximum efficiency and at the same Mach number: to keep these conditions the altitude is increased at each time step. In terms of computational costs, the cruise climb option is faster than the step climb, since the code does not check at each iteration if it is convenient to perform the step climb or not.

In order to assess the difference between the two approaches, the case of a cruise climb is performed, using the TLAR of the CeRAS aircraft[27] (2750NM of range for 150 passengers). The results have been compared with that reported by Schmollgruber et al.:[6] the differences shown in Table 5 are negligible. Thus in the following sizing loops presented in this paper the cruise climb option is always used.

Table 5. Comparison between the step climb and the cruise climb approaches, using the CeRAS aircraft[27] (N_{pax}=150, M=0.78, R=2750NM)

		Step climb	Cruise climb	Diff. %
MTOW	[kg]	74 618.96	74 562.82	−0.075
OWE	[kg]	42 200.58	42 190.71	−0.023
Wing area	[m^2]	122.74	122.68	−0.481
Fuel mission	[kg]	18 799.11	18 798.85	−0.001

Since an hybrid propulsion system is used, the degree of hybridization over the entire mission has to be defined: recalling Eq. (1), the battery power rate defines the use of the battery for each segment. Two cases are possible: the power is not balanced (i.e. for takeoff and climb) and it is balanced (i.e. in cruise). In the first case the battery and generator power rates are given in input, meanwhile in the second case only the percentage of power required by the battery is given in input, then the two power rates are computed. Batteries are never used in cruise, since the energy consumption leads to an increasing in weight that is not affordable for the aircraft. In order to be sure to use the batteries in the most efficient way, the SoC at the end of the mission has to be 20%: if at the end of the sizing the SoC is greater than this value, the degree of hybridization is manually changed until it is 20%.

B. Sizing parameters

For the sizing a certain number of TLAR have to be defined into the .xml input file. In Table 6 the design parameters for the hybrid aircraft are reported: the number of passengers is the same of an aircraft A320-type (150); the range varies from 800 to 1600NM, meanwhile the Mach number is 0.7, lower than a traditional aircraft. As said, the value of 0.7 has been chosen in order to reach a fan diameter that would be too small, as there is a limit due to technology level. About the propulsive architecture, 2 generators, 4 batteries and 40 engines have been considered; finally the minimum power required at takeoff is fixed to 28MW.

After having defined the TLAR, the parameters for the electrical components have to be chosen. As already mentioned, the focus is on the 2035 horizon: in bibliography there are different values for the chosen technological horizon (see for example the works of Lowry and Larminie,[19] Bradley and Droney,[8] Belleville,[29] Friedrich et al.,[30] Delahye,[31] as the HASTECS project[32] and the estimation of Fraunhofer Institute[18]). All the data found in bibliography are different, leading to an incertitude: after an internal discussion at ONERA and ISAE-Supaero the technology table reported in Table 7 has been defined. However, due to the aforementioned uncertainity in defining the technological horizon, sensibility analysis will be later shown with variation of the parameters in order to assess the effect.

Finally, due to the development of new materials, a reduction in the weight has to be considered. In Table 8 the estimated impacts of a 2035 technology on the weight of different components are reported: values come from an internal project at ONERA, in the frame of the EU program Clean Sky 2.[10]

Table 6. Design parameters for the hybrid aircraft with DEP considered

Range	800-1600	NM
Cruise Mach number	0.70	
Number of passengers	150	
Approach speed	132	kn
Wing span	$\leq$36	m
Number of engines	40	
Number of generators	2	
Number of batteries	4	
Minimum power at takeoff	28	MW

Table 7. Design parameters for the electric components for 2035 horizon

		Battery	**Generator**	**Electric motor**	**IDC**
Specific energy density	[W h kg^{-1}]	500	-	-	-
Energy density	[W h L^{-1}]	850	-	-	-
Specific power density	[kW kg^{-1}]	2.0	13.15	10.0	16.4
Power density	[kW L^{-1}]	3.4	-	20.0	-
Efficiency	[-]	0.90	0.95	0.95	0.95

Table 8. Estimated impact of new materials on weight for 2035 horizon

Wing	-10	%
Fuselage	-5	%
Landing gear	-5	%
Cabin seats	-30	%

The wing weight reduction is valid only for a conventional aircraft: it is not possible to use composites because of the level of current that flows in the cables in the wing. Thus, for the hybrid concept, no wing reduction is considered.

In the next section, where results are presented, the hybrid aircraft is compared with respect to a conventional aircraft: the last has the same TLAR reported in Table 6, the weight reduction reported in Table 8, a maximum efficiency of 19 is assumed and the engine model is based on the CeRAS engine,[27] with a SFC reduction of 20%.

VI. Preliminary results for the Hybrid-Electric Aircraft concept

As stated in the previous section (Table 6), the range is not fixed: in fact it is a variable to be explored in order to find the breaking point from which the hybrid concept is advantageous with respect to a traditional aircraft. The first parametric study shows the fuel consumption with respect to the range: the result is presented in Fig. 8. For both the configurations (conventional and hybrid) the fuel consumption increases with the range, but it is possible to note a value (about 1200NM) for which the two configurations have the same fuel consumption. Under that value the hybrid configuration is advantageous with respect to the traditional one. This effects is due to the battery sizing: under the breaking value, the sizing criteria is the power requirement at takeoff (which is 28MW), which means that the energy available is the same. When the range is decreased, the MTOW is decreased too, and this leads to a final SoC greater than 0.20: it is then possible to change the degree of hybridization and save more fuel. On the contrary, when the range is higher than 1200NM, the energy requirement becomes the most important criteria: batteries are resized and the increasing in weight make the hybrid architecture worse than the traditional one. For the rest of the work here

presented, the design range considered is 1200NM, with the mission hybridization reported in Table 9: since the battery is sized according the power requirements, there is more energy than needed for the mission fully electric until 3000ft; for this reason the entire climb segment is fully electric, with a battery power rate of 70%.

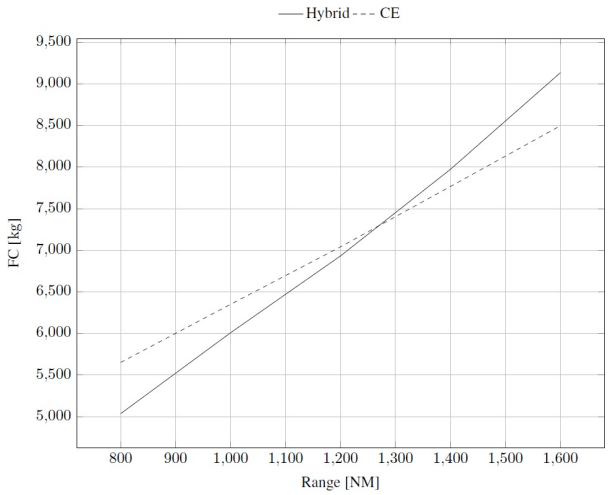

Figure 8. Fuel consumption with respect to the range variation, keeping constant all the others TLAR

Table 9. Different technological scenarios for evaluating the sensitivity to technology

	$\delta_{\mathbf{gen}}$	$\delta_{\mathbf{batt}}$
Takeoff & Initial climb	0.0	1.0
Climb	0.0	0.7
Cruise	comp.	0.0
Descent	0.3	0.0
Alternate climb	0.8	0.0
Alternate cruise	comp.	0.0
Alternate descent	0.3	0.0
Holding	comp.	0.0
Taxis segments	0.0	0.05

Table 10 shows the comparison for the two different configurations. In order to have a unique parameter for comparison, the Payload Fuel Energy Efficiency (PFEE) has been used as figure of merit.[33] This parameter is defined as the payload per range divided by the energy consummed:

$$PFEE = \frac{(PL)(Range)}{E_{cons}} \tag{18}$$

PFEE has been used since it contains the payload carried for a certain range, and the energy consummed for the mission. The PFEE is similar for both configurations, which confirms the results that for the chosen range the hybrid and the traditional aircraft are comparable (about $98\,\mathrm{kg\,km\,MJ^{-1}}$), but for the first concept there are no emissions close to ground.

The OEI condition is already included in the FAST calculation, but is not critical in the design. The cases in which one generator or two batteries are inoperative have been then considered as additional failure cases: the hypothesis made is that the failure occurs during takeoff. As explained in section II and section III, the aircraft is designed in order to have all the EM operative, even if one energy source is inoperative. The fuel breakdown for these cases is reported in Table 11. In case one generator is inoperative, there are

Table 10. Comparison between the Hybrid-Electric concept and the conventional aircraft, EIS2035, for the desired range of 1200NM

		Hybrid	Traditional	Diff. %
Wing area	[m^2]	118.77	105.92	12.13
Maximum L/D	[-]	17.2	19	10.46
Initial cruise altitude	[kft]	31	36	16.13
MTOW	[t]	80.08	57.20	40.01
OWE	[t]	59.50	36.55	62.79
Block fuel	[kg]	4750.26	4869 11	−2.44
Reserve fuel	[kg]	2182.22	2172 48	0.44
Mission fuel	[kg]	6932.49	7041 59	−1.55
Battery energy	[W h]	1806.90	-	-
PFEE	[kg km MJ^{-1}]	98.31	97.44	0.89

no differences in the takeoff and climb phase, since they are fully electric; then it is still possible to conclude the cruise, even if the fuel consumption is higher since more power is required to a single generator and the PSFC increases. For the reserve phase, the aircraft is not able to climb again for an alternate flight as the power requirement for this segment is higher than the maximum power of a generator, and only 45 minutes of holding have been considered. In case two batteries are out, instead, it is not possible to have a fully electric segment and the help of the generator is required at each phase. No great differences are shown for the reserve calculation, as for that phase only generators are used also in the baseline, but the fuel increases for the design flight.

This study has been performed in order to understand the behavior in case of failure, but it does not consider yet the possible certification requirements (i.e. that if one source is inoperative the aircraft has to climb to 500ft and then lands again); a detailed work has to be done in the future.

Table 11. Fuel breakdown comparison between the baseline and the scenarios of failure identified (one generator or two batteries inoperatives)

		No failure	Generator out	Batteries out
Taxi out	[kg]	0	0	0
Takeoff	[kg]	0	0	36.67
Initial climb	[kg]	0	0	118.52
Climb	[kg]	0	0	362.41
Cruise	[kg]	4543.81	4984.86	4857.90
Descent	[kg]	206.46	227.79	228.58
Alternate climb	[kg]	562.62	-	604.35
Alternate cruise	[kg]	325.39	-	365.10
Alternate descent	[kg]	156.98	-	172.68
Holding	[kg]	994.74	1102.73	1078.89
Block fuel	[kg]	4750.26	5212.65	5604.13
Reserve fuel	[kg]	2182.22	1259.11	2389.14
Mission fuel	[kg]	6932.49	6471.76	7993.27

VII. Exploration of the design space

The technology data for 2035 are affected by uncertainty. In order to assess the effects of a different technological level on the feasibility of the proposed concept, an exploration of the design space has been

performed in this section. Battery, generator, electric motor and gasturbine technologies variation have been considered, as the effects of the engines number (to assess the DEP advantages) and the maximum 2D lift coefficient variation. Table 12 reports the minimum and maximum values for the parameters of the hybrid chain components. Some assumptions have been made:

- The TLAR used are the same used in the previous section (Table 6).
- The effect of each component has been studied separately, changing one component's technology and keeping all the others constant and equal to the baseline (Table 7, and reported also in Table 12 for sake of clarity).
- The mission hybridization is the same used for the baseline (Table 9): in case at the end of a simulation the SoC is greater than 0.20 as required by equation (11), it has been changed in order to use all the available battery energy. Changes are always reported.

Table 12. Technology table for evaluating the sensitivity to technology

		Minimum	**Maximum**	**Baseline**
Battery specific energy density	[W h kg^{-1}]	350	700	500
Battery specific power density	[W kg^{-1}]	1400	2800	2000
Battery efficiency	[-]	0.85	0.95	0.9
Generator specific power density	[kW kg^{-1}]	6.57	19.72	13.15
Generator efficiency	[-]	0.90	0.97	0.95
Electric motor specific power density	[kW kg^{-1}]	5	15	10
Electric motor efficiency	[-]	0.90	0.98	0.95
Number of engines	[-]	10	40	40
Max C_l	[-]	4.0	5.0	4.5
Gasturbine PSFC variation	[%]	-10	10	0

For all the studies three key parameters have been considered as output: the MTOW, the wing area S_w and the fuel consumption FC. They have been chosen since they are the most important parameters in a design process. The results are presented in Fig. 10: each column represents the impact of one component's technology variation for the key parameters. The same scale has been used, in order to better understand the effect of a variation on a single output (MTOW, S_w and FC). In the next sections the impact of each parameter is described separately; for sake of clarity in Appendix C all the graphs are reported (from Fig. 14 to Fig. 19), both in the common and real scales.

A. Impact of battery technology variation

In this section the variation of battery technology in the range defined in Table 12 has been studied; results are shown in the first colume of Fig. 10. The battery technology affects all the parameters considered: between the minimum and the maximum value, the MTOW is reduced of about 20%, the wing area of about 15% and the fuel consumption of about 18%. It is possible to note that from the first and the second point (from an energy density of 350W h kg^{-1} to 500W h kg^{-1}) the MTOW is reduced more than in the second segment: this happens because, for low values of $\left(\frac{E}{m}\right)_{batt}$ batteries are resized accorgind to the energy requirement, leading to a divergence into the MTOW. In the last case ($\left(\frac{E}{m}\right)_{batt}$=700W h kg^{-1}), instead, the sizing criteria is the power at the takeoff, and since the MTOW is reduced of 8% with respect to the baseline, there is more energy to use in batteries and the degree of hybridization for the alternate climb is changed respect to what has been used in Table 9:

$$- \ \delta_{gen_{al,climb}} = 0.0$$

$$- \ \delta_{batt_{al,climb}} = 0.65$$

Thus, for the last point also the alternate climb is fully electric, leading to a major gain in fuel consumption.

B. Impact of generator technology variation

The generator technology is varied into the range identified in Table 12. Minimum and maximum values correspond to a variation of ±50% respect to the design. The results correspond to the second column of Fig. 10. The effects on the MTOW, wing area and fuel consumption are smaller, compared to that of the battery technology: the MTOW varies of about 4%, meanwhile the wing area is almost constant. The major effect is on the FC (about 7%): when the weight of the generator is decreased, the nacelle is smaller, and thus there is a little gain on the efficiency, which affects the FC.

C. Impact of electric motor technology variation

The variation of electric motor technology has then been studied, within the range presented in Table 12: as for the generator, minimum and maximum value of power to mass ratio have been defined considering a variation of ±50% with respect to power to mass ratio base value. Results are shown in the third column of Fig. 10: both on the MTOW and the fuel consumption there is a gain of about 7%, meanwhile the effect on the wing area is not relevant. The effects are greater than that of the generator technology variation, but still smaller than that of the battery technology variation.

D. Impact of engines number variation

In this section the effect of engines number has been considered: it varies from 10 to 40 (as reported in Table 12). This parameter affects the maximum lift coefficient. In fact, as said earlier, the surface interested by the blowing has a maximum C_l of about 4.5; the wing maximum C_L is computed as:

$$C_{L,wing_{max}} = C_{l,max} \frac{S_{blow}}{S_w} \tag{19}$$

where S_{blow} is the surface interested by blowing, shown also in Fig. 9 in red. From Eq. (19) it can be deduced that the maximum C_L is reduced when S_{blow} is reduced, that is when the engines number is smaller.

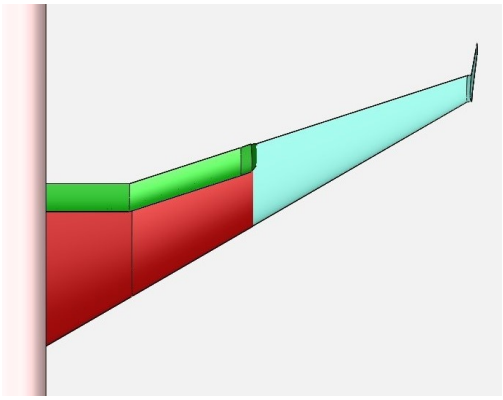

Figure 9. Wing view. The red zone represents the surface interested by blowing, used for computing the maximum lift coefficient in Eq. (19)

Results of this study correspond to the fourth column of Fig. 10: there are no relevant effect on the MTOW and FC, meanwhile the wing area changes of about the 20%. This is explained because the wing area is sized according the approach speed constraint, and when there are less engines the maximum C_L is smalled, and this leads to a greater wing area to sustain the flight.

E. Impact of maximum 2D lift coefficient effects

The effect of maximum 2D lift coefficient has been considered: as already said, it is estimated to vary between 4 and 5. Results are shown in the fifth column of Fig. 10. The only effect is on the wing area (which is reduced of the 15%): this means that the main advantages in having a higher C_l are not in the FC, but in the possibility to have a shorter takeoff field length and a smaller power at takeoff requirements (parameter that affects the battery sizing).

F. Impact of PSFC variation

Finally, the effects of PSFC variation have been considered: the value is first decreased by 10% and then increased by the same amount with respect to the baseline (as in Table 12). Results are shown on the last column of Fig. 10: the main effect is in the FC, which varies of the 20% in the range considered. The result is expected, since the PSFC mainly depends on the combustion process efficiency. The effect on the MTOW and the wing area is instead negligible (less than 1%).

These analyses show that, when the technologies improve, in general the performances are better (MTOW and fuel consumption are reduced), meanwhile the study on the number of engines clearly shows the advantage in using a DEP architecture. It is also possible to note that a linear change in a technology does not imply a linear change in the results: this happens because a reduction in the weight leads to a reduction in the energy consumption, and so in a reduction in battery weight (if it is sized according to energy) or in the fuel consumption (if it is sized according to power at takeoff, since more energy is available). In order to better understand the effects of each parameter, a sensitivity analysis has been performed, based on the method of the sparse polynomial chaos expansions, with a design of experiments made of 800 points. Fot its generation, a Latin Hybercube Sampling has been used. The idea is to identify the sensitivity index of the three key parameters (MTOW, S_w and FC) with respect to the design variables, in order to understand the impact of each variable on a certain output. It is also possible to identify the interaction between the variables, if there are.

VIII. Sensitivity studies with respect to technological levels

The analysis performed is based on the sparse polynomial chaos expansions method for computing global sensitivity indices.[34,35] This method has been selected since it allows to compute the sensitivity (Sobol) indices as the Montecarlo method, but it requires less points for the estimation. In this section it is assumed that $Y = \mathcal{M}(X)$, where $X = (X_i),\ i = 1, \cdots, n$ (n being the number of design variables), is a random vector modeling the input parameters (independent and uniformly distributed) and $\mathcal{M}$ is the numerical solver used to compute a scalar quantity of interest Y (the sizing tool FAST in this work). Assuming that Y is a second order random variable, it can be shown that[36]

$$Y = \sum_{i=0}^{\infty} C_i \phi_i(X) \tag{20}$$

where $\{\phi_i\}_{i\in\mathbb{N}}$ is a polynomial basis orthogonal with respect to the probability density function (pdf) of X and C_i are unknown coefficients. Sparse polynomial chaos consists in the construction of a sparse polynomial basis $\{\phi_i\}_{\alpha\in\mathcal{A}}$, where $\alpha = (\alpha_1, \cdots, \alpha_n)$ is a multi index used to identify the polynomial acting with the power α_i on the variable X_i and $\mathcal{A}$ is a set of index α. In practice $\mathcal{A}$ is a subset of the set $\mathcal{B}$ which contains all the index α up to a dimension d *i.e.* $card(\mathcal{B}) = \frac{(d+n)!}{d!n!}$. Objective of sparse approach is to find an accurate polynomial basis $\{\phi_i\}_{\alpha\in\mathcal{A}}$ such as $card(\mathcal{A}) << card(\mathcal{B})$. This is achieved by Least Angle Regression *i.e.* unknown coefficients C_i are computed by iteratively solving a mean square problem and selecting, at each iteration, the polynomial the most correlated with the residual.[37] Finally, the following approximation is deduced:

$$Y \approx \hat{Y} = \sum_{\alpha\in\mathcal{A}} C_\alpha \phi_\alpha(X) \tag{21}$$

Due to the orthogonality of the polynomial basis $\{\phi_i\}_{\alpha\in\mathcal{A}}$ it is possible to write:

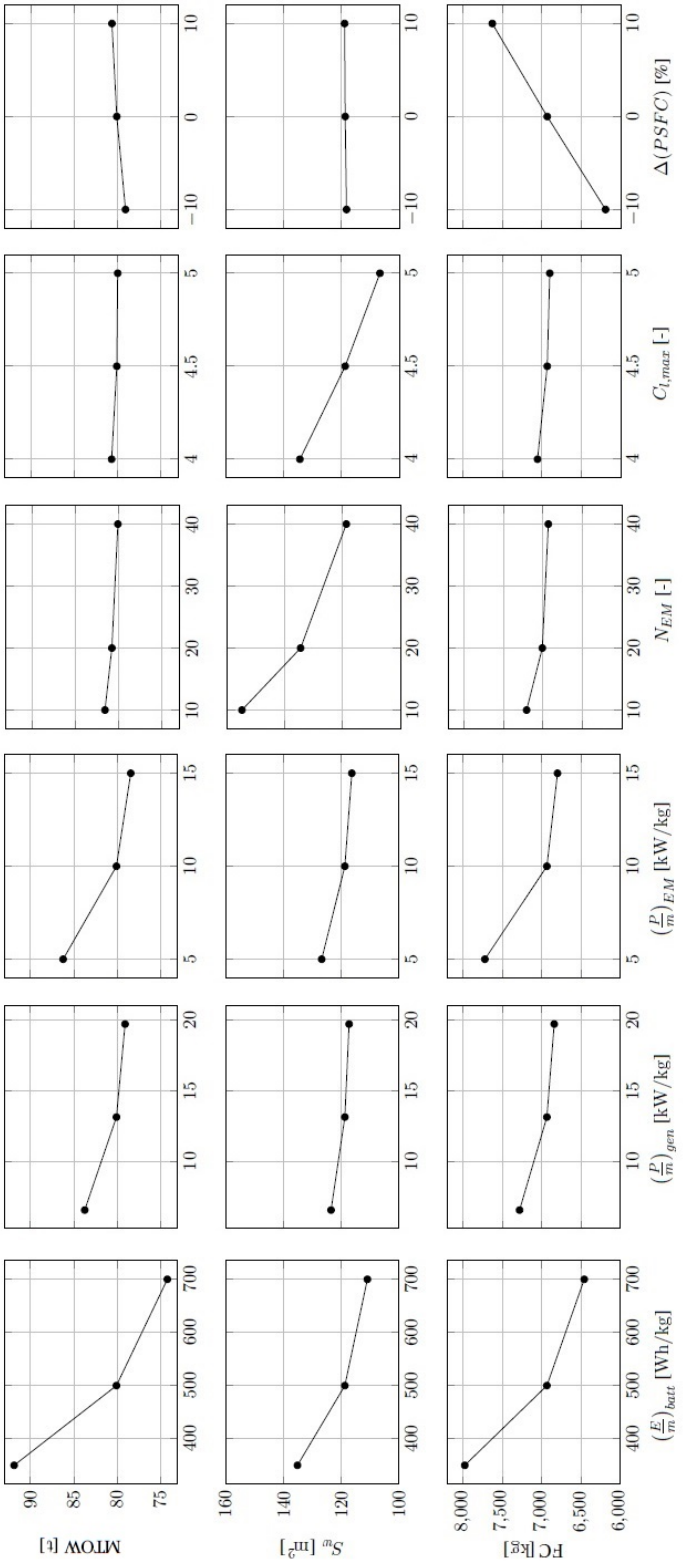

Figure 10. Parametric analysis results: each column represents the effect of the variation of a component's technology, keeping constant all the other. The first column represents the impact of the battery, the second column the impact of the generator, the third column the impact of the electric motors, the fourth the impact of the number of engines, the fifth the impact of the maximum 2D lift coefficient, and the sixth the effect of the PSFC reduction. The output considered are the MTOW, the wing (S_w) area and the fuel consumption (FC)

$$\begin{cases} E[\hat{Y}] = C_0 \\ Var[\hat{Y}] = \sum_{\alpha \in \mathcal{A}} C_\alpha^2 E[\phi_\alpha^2(X)] \end{cases} \tag{22}$$

where $E[\hat{Y}]$ is the mean value and $Var[\hat{Y}]$ is the variance of the answered variable ($\hat{Y}$).

Sudret[38] identifies the polynomial chaos expansion using the ANOVA decomposition, from which it is possible to show that the **first order sensitivity index** of the variable X_i is

$$\hat{S}_i = \frac{\sum_{\alpha \in L_i} C_\alpha^2 E[\phi_\alpha^2(X)]}{Var[\hat{Y}]} \tag{23}$$

where $L_i = \{\alpha \in \mathcal{A} / \forall\ j \neq i\ \alpha_j = 0\}$; that is only the polynomials acting exclusively on variable X_i have been considered.

The **total sensitivity index** can also be computed:

$$\hat{S}_{T_i} = \frac{\sum_{\alpha \in L_i^+} C_\alpha^2 E[\phi_\alpha^2(X)]}{Var[\hat{Y}]} \tag{24}$$

where $L_i^+ = \{\alpha \in \mathcal{A} / \alpha_i \neq 0\}$; that is all the polynomials acting on the variable X_i have been considered (which means that all variance caused by its interaction, of any order, with any other input variables are included).

The idea is to determine the sensitivity indices relative to the technology component used in FAST for the MTOW, the S_w and the FC. From the analysis the same parameters considered in Table 12 have been considered, except for the battery specific power density (which from the table can be estimated to be 4 times the specific energy density) and the number of engines (since this method only considers continuous variables). For each variable it is possible to define the coefficient of variation CV:

$$CV = \frac{\sigma}{\mu} \tag{25}$$

where $\sigma = \sqrt{\frac{(x_{max} - x_{min})^2}{12}}$ is the variance and $\mu = \frac{x_{max} - x_{min}}{2}$ the mean value. It has been decided to work keeping constant the CV for each variable: once that the mean value is fixed, it is possible to deduce the minimum and maximum values of variation. In Table 13 the mean values and the range of variation for each parameter are reported. It has to be noted that, compared to Table 12, the range of variation is smaller.

Table 13. Mean values, minimum and maximum values for the parameters considered for the sensitivity analysis (with CV=0.05 kept constant for all the variables).

		Mean value	**Minimum**	**Maximum**
Battery specific energy density	[W h kg^{-1}]	500	456.70	543.30
Battery efficiency	[-]	0.9	0.82	0.97
Generator power density	[kW kg^{-1}]	13.15	12.01	14.29
Generator efficiency	[-]	0.9	0.82	0.97
EM power density	[kW kg^{-1}]	10	9.13	10.86
EM efficiency	[-]	0.9	0.82	0.97
$C_{l,max}$	[-]	4.5	4.11	4.89
PSFC reduction	[%]	0	−8.66	8.66

A database of 800 points has been generated for the experiment (via a Latin Hypercube Sampling). The coefficient of variation used is 0.05 (which means that each variable changes of 5% between the minimum and maximum value). Results are shown in Table 14 and Fig. 11. The following conclusions can be deduced:

- MTOW is mostly affected by the battery technology (which has a sensitivity index of 0.86).

- The driving parameter for the FC is the PSFC reduction (sensitivity index is 0.64), but there is also an effect of the battery, due to the fact that when it is resized, the MTOW increases and so the FC. Also the EM efficiency has an effect: recalling the propulsive chain (Fig. 3), this parameter regulates the power required by generators, which affects the FC (with the same PSFC, more power means more fuel burnt).
- The wing area is finally driven by the maximum 2D lift coefficient (sensitivity index is 0.84); also for this parameter there is a small effect of the battery technology, due to the fact that the sizing criteria for the wing is the approach speed, and when the MTOW increases, a greater area is needed to sustain the flight.

From Table 14 it is also possible to note that the sum of all the indices is about one (from 0.99 to 1.07): this means that all the variance of the answered variables is explained, and there are no high order interactions between the input variables. Thus a study of the total sensitivity indices does not provide more information than the first order indices. (see Eq. (24)).

Table 14. Sensitivity indices for MTOW, FC and S_w for the analysis considered (in bold the relevant values)

	MTOW	**FC**	**S_w**
Battery specific energy density	**0.8642**	0.1799	0.1561
Battery efficiency	0.0002	0.0000	0.0000
Generator power density	0.0126	0.0561	0.0010
Generator efficiency	0.0004	0.0001	0.0000
EM power density	0.0001	0.0086	0.0000
EM efficiency	0.1070	0.1848	0.0003
$C_{l,max}$	0.0119	0.0089	**0.8421**
PSFC reduction	0.0003	**0.6389**	0.0000
Index sum	0.9968	1.0773	0.9995

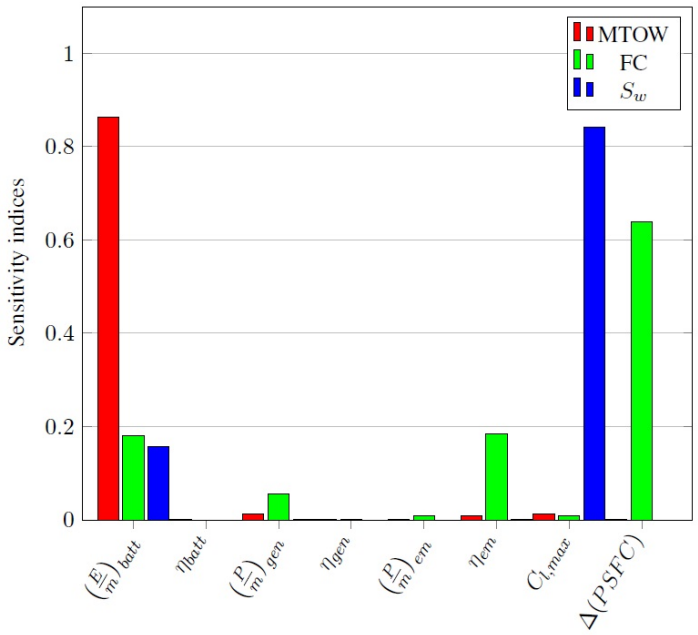

Figure 11. Plot of sensitivity indices for MTOW, FC and S_w for the analysis considered.

Having fixed the CV, the range in which the parameters vary is smaller than the technological range established in Table 12. For this reason a second analysis has been performed, using the assumption made in the technological table (which means that the CV is not the same for each parameter anymore). A new database of 800 points has been defined. Results are presented in Table 15 and Fig. 12. Compared to the previous case, the effects are mostly due to the battery variation, except for the wing area, for which there is still an effect of the maximum lift coefficient, even if it is reduced. This means that, until the uncertainty in battery technology is as it has been hypotized, there is no gain in improving the technological level of the other components, since the sizing will be affected mostly by the battery parameters.

Table 15. Sensitivity indices for MTOW, FC and S_w, considering the range of variation defined in Table 12 (in bold the relevant values)

	MTOW	**FC**	**S_w**
Battery specific energy density	**0.9358**	**0.7388**	0.3792
Battery efficiency	0.0000	0.0001	0.0000
Generator power density	0.0569	0.0561	0.0223
Generator efficiency	0.0002	0.0001	0.0002
EM power density	0.0017	0.0086	0.0004
EM efficiency	0.0032	0.1848	0.0005
$C_{l,max}$	0.0015	0.0089	**0.5953**
PSFC reduction	0.0000	0.0026	0.0000
Index sum	0.9992	0.9975	0.9974

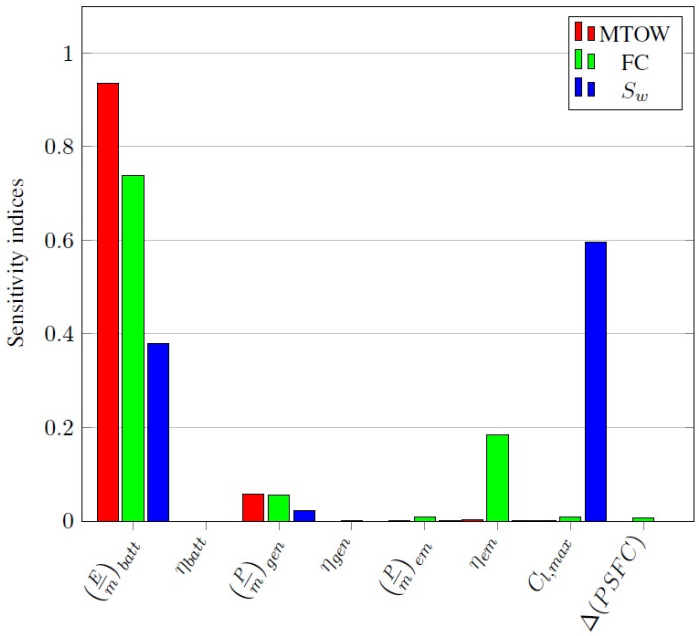

Figure 12. Plot of sensitivity indices for MTOW, FC and S_w, considering the range of variation defined in Table 12

In conclusion, with the current level of fidelity used in FAST, it is possible to consider the effects of the technology variation; results shown that the main driver for the design process is the battery.

IX. Conclusion & future perspectives

In this work the feasibility of a large passenger hybrid aircraft has been studied, in which a set of batteries and generators work in sinergy in order to supply power. The proposed concept is based on a distributed electric propulsion architecture, in which a certain number of ducted fans located along the wing provide the thrust necessary. A focus has been made on the advantages of such architecture (weight engine reduction due to the less stringent OEI condition, blowing effects which increase the maximum lift coefficient). Some efforts have been also made in electrical components' modeling and into the description of the propulsive energy chain. The technological hypotheses made refer to a 2035 horizon. All these aspects have been coded into the FAST sizing tool and the modifications made have been presented. The sizing tool is based on empirical equations and low fidelity tool: its level of fidelity can be classified as low.

Results show that the hybrid concept has a potential gain up to a certain range, after which the batteries weight become so large that the fuel consumption is increased compared with an aircraft with conventional engines, for the same technological horizon. Once that the baseline has been assessed, two failure cases (for batteries and generator) have been studied in order to understand if the aircraft can prevent the partial loss of one power source. A major investigation in the failure cases has to be considered in the future, according to new certification that could require to not be able to fullfill all the mission: in that case particular attention has to be put into the maximum power can be lost. Also, in the proposed concept the assumption that all electric motors work even if there is a energy source loss has been made: the case in which a loss of a energy source lead to a loss of a certain number of engines (which affects the maximum wing lift coefficient) has to be considered too. However, the scenarios considered in this work are conservative in that sense.

Due to the uncertainity in the data for the 2035 horizon, an exploration of the design space, with the technology table available, and sensitivity analyses have been performed. The tradeoff shows that the main parameter for the design process is the battery technology, with the PSFC reduction and maximum 2D lift coefficient having minor effects on the FC and wing area. The conclusion of this analyses is that, until the uncertainty into the battery technology holds, an improving in others components' technologies does not affect the results in a relevant way.

From an analysis point of view, FAST performs a MDA: this means that it reaches a viable aircraft, which is not necessary the optimum one (respect to fuel consumption). Next step is to bring the sizing loop here described into a MDO framework. This work can be divided into different phases:

- First step is to choose a MDO framework and include the sizing loop into an optimization loop, in order to find the set of TLAR and hybridization degree which minimize the energy and fuel consumption. A suitable choice for the MDO framework could be OpenMDAO, an open software developed by NASA Glenn Research Centre, in collaboration with University of Michigan.[39]
- FAST is a tool based on a low fidelity level. A second step is then to study different fidelity levels in FAST in order to assess the difference in results using multifidelity tools. These first two steps considering different scenarios only regarding the battery technology.
- Finally, in order to better understand the effect of the technology level, a MDO formulation using uncertainty quantification could be derived.[40]

Acknowledgments

The authors would like to thank:

- AIRBUS for the financial support in the frame of Chair CEDAR (Chair for Eco Design of AircRaft).
- The European Commission for the financial support within the frame of the Joint Technology Initiative JTI Clean Sky 2, Large Passenger Aircraft Innovative Aircraft Demonstration Platform "LPA IADP" (contract N CSJU-CS2-GAM-LPA-2014-2015-01).
- Michael Ridel and David Donjat for their contribution on cables and cooling system models as well as Sylvain Dubreuil for his work on the sensitivity analysis.

References

[1]ACARE project, http://www.acare4europe.com/sria

[2]F. Collier and R. Wahls, *ARMD Stsrategic Thrust 3: Ultra-efficient Commercial Vehicles Subsonic Transport*, Washington DC, 24 May 2016

[3]R. Kirner, *An Investigation into the Benefits of Distributed Propulsion on Advanced Aircraft Configurations*, Ph.D. thesis, Cranfield University, 2014

[4]A. Ko, J.A. Schetz and W.H. Mason, *Assessment of the Potential Advantages of Distributed Propulsion for Aircraft*, International Society for Air Breathing Engines, ISABE-2003-1094, 2003

[5]E.M. Greitzer, P.A. Bonnefoy, E. De la Rosa Blanco, C.S. Dorbian, M. Drela, D.K. Hall, R.J. Hansman, J.I. Hileman, R.H. Liebeck, J. Lovegren, P. Mody, J.A. Pertuze, S. Sat, W.S. Spakovszky, C.S. Tan, J.S. Hollman, J.E. Duda, N. Fitzgerald, J. Houghton, J.L. Kerrebrock, G.F. Kiwada, D. Kordonowy, J.C. Parris, J. Tylko, E.A. Wen and W.K/ Lord, *N+3 Aircraft Concept Design and Trade Studies, Final Report, vol.s 1&2*, NASA/CD-2010-216794/VOL1-VOL2, 2010

[6]P. Schmollgruber, J. Bedouet, A. Sgueglia, S. Defoort, R. Lafage, N. Bartoli, Y. Gourinat and E. Benard, *Use of a Certification Constraints Module for Aircraft Design Activities*, 17th AIAA Aviation, Technology, Integration and Operations Conference, Denver, Colorado, 5-9 June 2017

[7]OpenVSP tool, http://www.openvsp.org

[8]M.K. Bradley and C.K. Droney, *Subsonic Ultra Green Aircraft Research: Phase II-VolumeII-Hybrid Electric Design Exploration*, NASA/CR-2015-218704/Volume II

[9]A.T. Wick, J.R. Hooker, C.J. Hardin and C.H. Zeune, *Integrated Aerodynamic Benefits of Distributed Propulsion*, 53rd AIAA Aerospace Sciences Meeting, AIAA SciTech Forum, Kissimee, Florida, 5-9 January 2015

[10]CleanSky Project, http://www.cleansky.eu/

[11]H.-J. Steiner, P.C. Vranty, C. Gologan, K. Wieczorek, A.T. Isikveren and M. Hornung, *Performance and Sizing of Transport Aircraft Employing Electrically-Powered Distributed Propulsion*, Deutscher Luft- und Raumfahrtkongress, Berlin, Germany, 2012

[12]Y. Li, J. Deng, C. Mu, Z. Xing and K. Du, *Vertical Distribution of CO_2 in the Atmospheric Boundary Layer: Characteristics and Impact of Meteorological Variables*, Atmosperic Environment, Elsevier, Volume 91, July 2014

[13]C. Pornet, A. Seitz, A.T. Isikveren and M. Hornung, *Methodology for Sizing and Performance Assessment of Hybrid Energy Aircraft*, Journal of Aircraft, January 2014. doi:10.2514/1.C032716

[14]G. Cinar, D.N. Mavris, M. Emeneth, A. Schneegans and Y. Fefermann, *Sizing, Integration and Performance Evaluation of Hybrid Electric Propulsion Subsystem Architectures*, 55th AIAA Aerospace Sciences Meeting, Grapevine, Texas, 9-13 January 2017

[15]R. Seresinhe and C. Lawson, *Electrical Load-Sizing Methodology to Aid Conceptual and Preliminary Design of Large Commercial Aircraft*, Journal of Aerospace Engineering, vol. 229(3), pp. 445-466, 2015

[16]W.P.J. Visser and M.J. Broomhead, *GSP: A Generic Object-Oriented Gas Turbine Simulation Environment*, NLR, NLR-TP-2000-267

[17]S. Burguburu and P.-M. Basset, *Turboshaft Engine Presedesign and performance Assessment*, 48th AIAA/ASME/SAE/ASEE Joint Propulsion Conference & Exhibit, Atlanta, Georgia, 30 July-1 August 2012

[18]Fraunhofer Institute for Systems and Innovation Research ISI, *Technology Roadmap Energy Storage for Electric Mobility 2030*, http://www.isi.fraunhofer.de/isi-wAssets/docs/t/en/TRM-ESEM-2030_en_web.pdf

[19]J. Lowry and J. Larminie, *Electric Vehicle Technology Explained*, John Wiley & Sons, 2nd edition, 2012

[20]G. Cinar, D.N. Mavris, M. Emeneth, A. Schneegans and Y. Fefermann, *Development of a parametric Power Generatin and Distribution Subsystem Models at Conceptual Aircraft Design Stage*, 55th AIAA Aerospace Sciences Meeting, Grapevine, Texas, 9-13 January 2017

[21]Ampere (Avion Motorisation réPartie Électrique de Recherche Epérimentale) project, https://www.onera.fr/sites/default/files/actualites/breves/Fiche_AMPERE_VA.pdf

[22]F. Anton, *High-output Motor Technology for Hybrid-Electric Aircraft*, eAircraft Electric & Hybrid Aerospace Technology Symposium, Cologne, Germany, 16th November 2017

[23]S.F. Hoerner, *Fluid-Dynamic Drag - Theoretical, Experimental and Statistical Information*, published by the author, 1965

[24]*Catalogue NORMES Défense 2016*, Direction Générale de L'Armement (DGA), Ministre de la Défense Française, 2016

[25]A.B. Lambe and J.R.R.A. Martins, *Extensions to the Design Structure Matrix for the Description of Multidiplinary Design, Analysis, and Optimization Processes*, Structural and Multidisciplinary Optimization, vol. 45, no. 2, pp.273-284, 2012

[26]W.P. Dupont and C. Colongo, *Preliminary Design of a Commercial Transport Aircraft*, class notes, ISAE-Supaero&Airbus, English edition, 2014

[27]CeRAS - Central Reference Aircraft Data System, https://ceras.ilr.rwth-aachen.de/

[28]M.K. Bradley and C.K. Droney, *Subsonic Ultra Green Aircraft Research: Phase I Final Report*, NASA, NASA/CR-2011-216847, 2011

[29]M. Belleville, *Simple Hybrid Propulsion Model for Hybrid Aircraft Design Space Exploration*, MEA - More Electric Aircraft conference, Toulouse, France, Febraury 2017

[30]C. Friedrich and P. Robertson, *Hybrid-Electric Propulsion for Aircraft*, Journal of Aircraft, vol. 52, n. 11, January 2015

[31]J. Delhaye, *Electrical Technologies for Aviation of the Future*, Airbus, 2015

[32]HASTECS project: programme de recherche aéronautique européen mené par le Laplace, http://www.inp-toulouse.fr/fr/la-recherche/l-excellence-autrement/l-actualite-recherche/hastecs.html

[33]J.I. Hileman, J.B. Katz, J.G. Mantilla and G. Fleming, *Payload Fuel Energy Efficiency as a Metric for Aviation Environmental Performance*, 26th International Congress of the Aeronautical Sciences, Alaska, 14-19 September 2008

[34]G. Blatman and B. Sudret, *Efficient Computational of Global Sensitivity Indices Using Sparse Polynopmial Chaos Expansions*, Reliability Engineering & System Safety, 95(11):1216-1229, 2010

[35]S. Dubreuil, M. Bervellier, F. Petutjean and M. Salaün, *Construction of Bootstrap Confidence Intervals on Sensitivity Indices Computed by Polynomial Chaos Expansion*, Reliability Engineering & System Safety, 121(Supplement C):263-275, 2014

[36]R.H. Cameron and W.T. Martin, *The Orthogonal Development of Non-Linear Functionals in Series of Fourier-Hermite Functionals*, Annals of Matehmatics, 48(2):385-392, 1947

[37]G. Blatman and B. Sudret, *Adaptive Sparse Polynomial Chaos Expansion Based on Least Angle Regression*, Journal of Computational Physics, 230(6):2345-2367, 2011

[38]B. Sudret, *Global Sensitivity Analysis Using Polynomial Chaos Expansions*, Reliability Engineering & System Safety, 98(7):964-979, 2008; Bayesian Networks in Dependability

[39]OpenMDAO software, `http://openmdao.org/`

[40]L. Brevault, M. Balesdent, N. Bérend and R. Le Riche, *Decoupled MDO formulation for interdisciplinary coupling satisfaction under uncertainty*, AIAA Journal, Vol.54(1): 186-205, DOI: 10.2514/1.J054121, 2016

A. Mass breakdown standard

As mentioned in section IV, the mass breakdown standard used in FAST is based on the French norm AIR 2001/D. The detailed mass breakdown is reported in Table 16: the aircraft has been divided into five categories: airframe, propulsion, systems and fixed installation, operational items and crew, plus fuel weight and payload. Each category has been divided into other subsections, one for each component, as clearly shown in the table. In category B, the sections B4, B5, B6, B7 and B8 have been added in order to consider the hybrid architecture too.

Table 16. Standard for mass breakdown used in FAST

A	**Airframe**
A1	Wing
A2	Fuselage
A3	Horizontal and Vertical tail
A4	Flight controls
A5	Landing gear
A6	Pylons
A7	Paint
B	**Propulsion**
B1	Engines
B2	Fuel and oil systems
B3	Unusable oil and fuel
B4	Cables and cooling system
B5	Batteries
B6	Generators
B7	IDC
B8	Bus protection
C	**Systems and fixed installations**
C1	Power systems (APU, electrical and hydraulical system)
C2	Life support systems (Pressurization, de-icing, seats, ...)
C3	Instrument and navigation
C4	Transmissions
C5	Fixed operational systems (radar, cargo hold mechanization)
C6	Flight kit
D	**Operational items**
E	**Crew**
F	**Fuel**
G	**Payload**

B. Methodology of preliminary design of a ducted fan

In this section the methodology used for the sizing of a ducted fan is explained. The scheme of the fan is shown in Fig. 13. Knowing the operating condition and the compressor ratio, it is possible to deduce the power required and then the size of the inlet and outlet area.

The input for the model are:

- Gas constants for the air: γ=1.4 and R=287J kg^{-1} K^{-1};
- Mach number in flight M_0

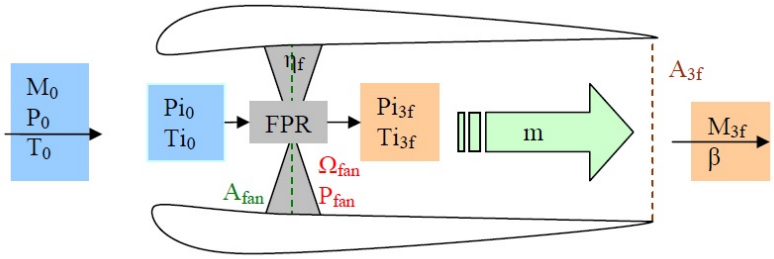

Figure 13. Scheme of a ducted fan for the model presented

- Altitude z, from which it is possible to deduce the static pressure and temperature p_{s0} and θ_{s0};
- The fan pressure ratio FPR, defined as the ratio between the total pressure at the exit and at the inlet of the fan;
- A reference surface S_{ref}, typically the wing surface;
- The non-dimensional thrust coefficient of one fan, defined as

$$C_T = \frac{T}{\frac{\gamma}{2} p_{s0} M_0^2 S_{ref}}$$

It has to be noted that the thrust coefficient is referred to the thrust required by a single ducted fan, and not the total thrust. The process is described below.

1. The first step is to compute the total pressure and temperature at the inlet, using the de Saint-Venant relations:

$$p_{t0} = p_{s0} \left(1 + \frac{\gamma - 1}{\gamma} M_0^2\right)^{\frac{\gamma}{\gamma - 1}}$$

$$\theta_{t0} = \theta_{s0} \left(1 + \frac{\gamma - 1}{\gamma} M_0^2\right)$$

2. Then it is possible to compute the Mach number at the exit of the nozzle:

$$M_{3f} = \sqrt{\frac{2}{\gamma - 1} \left[\left(1 + \frac{\gamma - 1}{\gamma} M_0^2\right) \mathrm{FPR}^{\frac{\gamma - 1}{\gamma}} - 1\right]} = f(M_0, \mathrm{FPR})$$

This relation is obtained considering the nozzle adapted, that is the pressure at the exit of the nozzle is equal to the ambient pressure ($p_{3f} = p_{s0}$). It is also possible to compute the velocity ratio β as follows:

$$\beta = \frac{V_{3f}}{V_0} = \frac{M_{3f}}{M_0} \sqrt{\frac{\theta_{3f}}{\theta_0}} = \frac{M_{3f}}{M_0} \sqrt{\mathrm{FPR}^{\frac{\gamma - 1}{\gamma}} \frac{1 + \frac{\gamma - 1}{2} M_0^2}{1 + \frac{\gamma - 1}{2} M_{3f}^2}} = f(M_0, \mathrm{FPR})$$

η_f being the polytropic efficiency of the fan. This value is introduced considering the ratio between the total pressure and the total temperature through the fan:

$$\frac{\theta_{t3f}}{\theta_{t0}} = \left(\frac{p_{t3f}}{p_{t0}}\right)^{\frac{\gamma - 1}{\gamma \eta_f}}$$

If η_f=1 the compression is isentropic. In practice it is possible to compute the polytropic efficiency with the semiempirical relation:

$$\eta_f = 0.98 - 0.08\,(\mathrm{FPR} - 1)$$

which take into account the effect of the FPR: the higher is, the less the compression is efficient.

3. At this stage it is possible to compute the nozzle exit area:

$$\frac{S_{3f}}{S_{ref}} = \frac{C_T}{2}\mathrm{FPR}^{\frac{\gamma(1-\eta_f)-1}{\gamma\eta_f}}\left(\frac{1+\frac{\gamma-1}{2}M_0^2}{1+\frac{\gamma-1}{2}M_{3f}^2}\right)^{\frac{1}{\gamma-1}}\frac{1}{\beta^2-\beta} = f(M_0, \mathrm{FPR}, C_T)$$

Finally, supposing the section circular, it is possible to deduce the diameter:

$$D_{3f} = 2\sqrt{\frac{A_{3f}}{\pi}}$$

4. At this step it is possible to compute the mass flow and then the power required by the fan. The mass flow which exits from the nozzle is:

$$\dot{m} = p_{3f}M_{3f}S_{3f}\sqrt{\frac{\gamma}{R\theta_{3f}}} = p_{3f}M_{3f}S_{3f}\sqrt{\frac{\gamma}{R\theta_{t3f}}}\left(1+\frac{\gamma-1}{2}M_{3f}^2\right)^{\frac{1+\gamma}{2(1-\gamma)}}$$

with $p_{t3f} = p_{t0}\mathrm{FPR}$ from the fan pressure ratio definition and $T_{t3f} = T_{t0}\mathrm{FPR}^{\frac{\gamma-1}{\gamma\eta_f}}$.
The total enthalpy variation is then

$$\Delta H = c_p(\theta_{t3f} - \theta_{t0}) = \frac{\gamma R}{\gamma-1}\theta_{t0}\left(FPR^{\frac{\gamma-1}{\gamma\eta_f}} - 1\right)$$

and finally the power required by the fan is

$$P_{fan} = \Delta H\dot{m}$$

5. It is finally possible to compute the fan area. For aerodynamic reasons, the Mach number at the fan section is 0.65, with this assumption the area is computed from the mass flow and the total conditions as

$$S_{fan} = \frac{\dot{m}}{p_{t0}M_{fan}\sqrt{\frac{\gamma}{R\theta_{t0}}}\left(1+\frac{\gamma-1}{2}M_{fan}^2\right)^{\frac{1+\gamma}{2(1-\gamma)}}}$$

Knowing then the ratio between the hub and tip radius σ, it is possible to compute the fan radius:

$$r_{fan} = \sqrt{\frac{S_{fan}}{\pi(1-\sigma^2)}}$$

6. Once the fan is sized, it is possible to deduce the rotational velocity and the torque. In order to do that, a tip velocity has to be defined: this value is determined by aerodynamic criteria and it allows to obtain the polytropic fan efficiency desired. Some values are summed up in the table below: it is possible to interpolate the data for different values of FPR.

Table 17. Tip velocity for different values of FPR

FPR	1.1	1.2	1.3	1.4	1.5	1.6	1.7	1.8
V_{tip} [$\mathrm{m\,s^{-1}}$]	200	230	290	330	370	390	400	400

The rotational speed, in round per minute, is then:

$$\Omega_{fan} = \frac{V_{tip}}{r_{fan}} \frac{60}{2\pi}$$

and finally the torque, in N m, is

$$C_{fan} = \frac{P_{fan}}{\Omega_{fan} \frac{2\pi}{60}}$$

The process just described has an error estimated of about 10%. It is still valid for off design conditions, the only difference is that a different value of FPR has to be found, in order to provide the same S_{3f}. In practice a lower FPR corresponds to a lower RPM on a real fixed-pitch fan. This is automatically done in the code.

C. Parametric analysis results

In this section the detailed results for the design space exploration (presented in Section VII) are reported. As explained, each study refers to a variation of only one technology, keeping all the others constant to the base values (Table 12). The results are shown in a real and a normalized scale (the same used in Fig. 10), in order to better understand the overall effect of each variation.

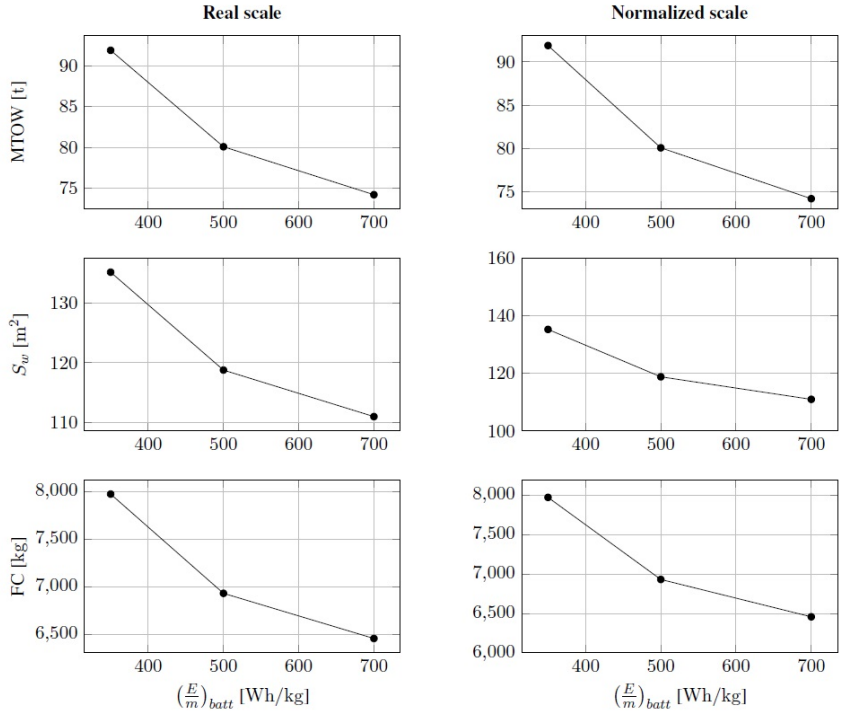

Figure 14. Parametric analyses with respect to battery technology. (E/m) is the battery specific energy density, MTOW the Maximum TakeOff Weight, S_w the wing area and FC the fuel consumption

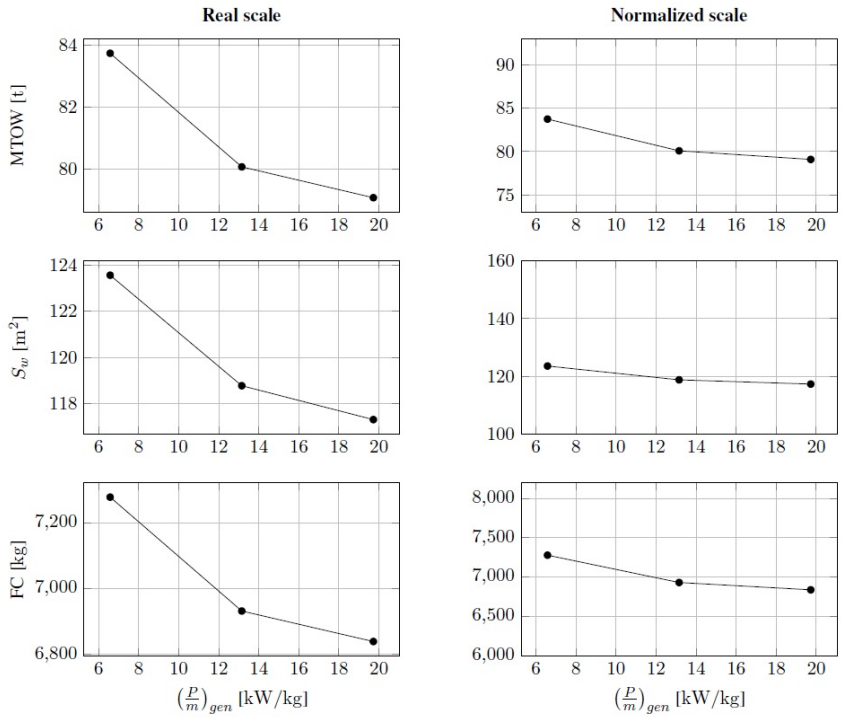

Figure 15. Parametric analyses with respect to generator technology. (P/m) is the generator specific power density, MTOW the Maximum TakeOff Weight, S_w the wing area and FC the fuel consumption

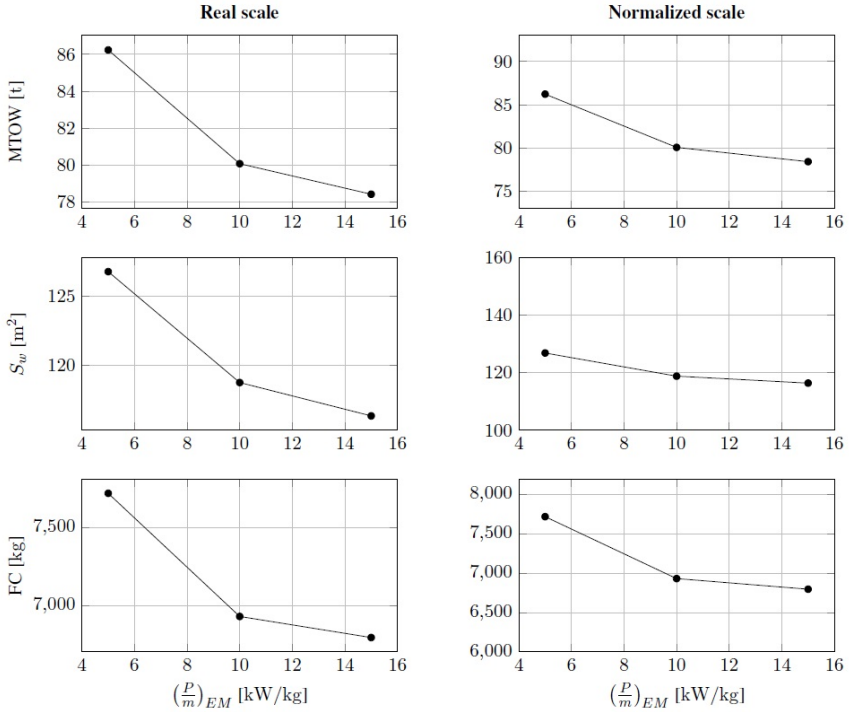

Figure 16. Parametric analyses with respect to electric motors technology. (P/m) is the electric motor specific power density, MTOW the Maximum TakeOff Weight, S_w the wing area and FC the fuel consumption

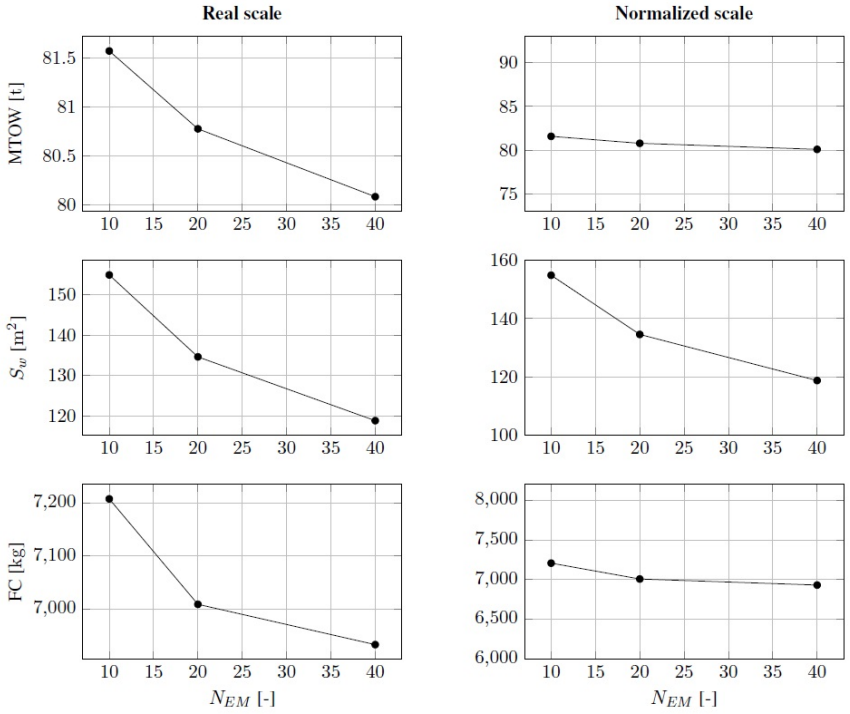

Figure 17. Parametric analyses with respect to the number of engines. N_{EM} is the number of engines (10, 20 and 40), MTOW the Maximum TakeOff Weight, S_w the wing area and FC the fuel consumption

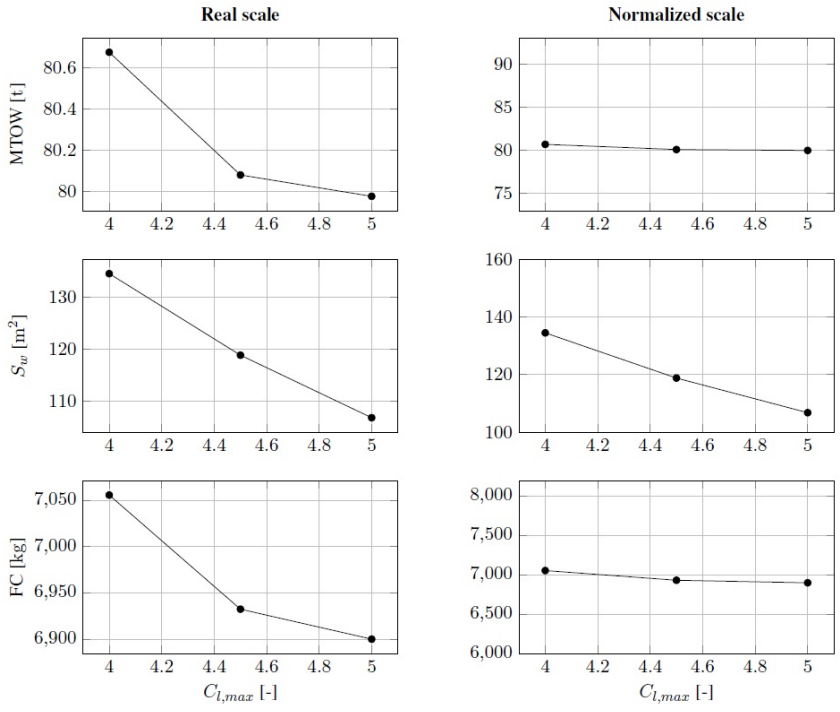

Figure 18. Parametric analyses with respect to maximum 2D lift coefficient. $C_{l,max}$ is the maximum 2D lift coefficient (4, 4.5 and 5), MTOW the Maximum TakeOff Weight, S_w the wing area and FC the fuel consumption

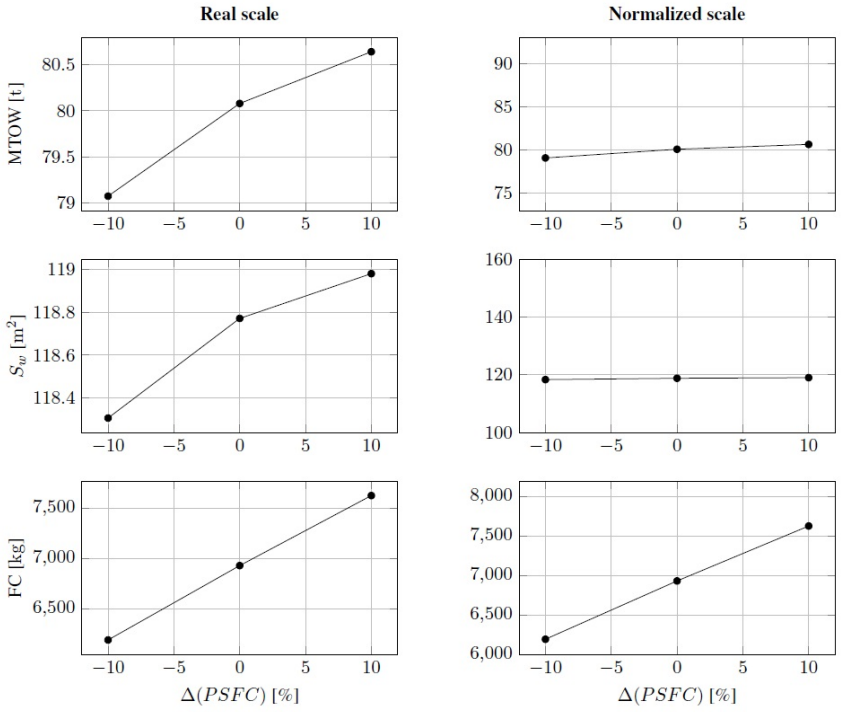

Figure 19. Parametric analyses with respect to PSFC variation. Δ(PSFC) is the PSFC reduction (-10%, 0% and +10%), MTOW the Maximum TakeOff Weight, S_w the wing area and FC the fuel consumption